

1                   **Supplementary Information**  
2  
3  
4

5                   **Effect of climate warming on the timing of autumn leaf senescence reverses**  
6                   **at the summer solstice**  
7  
8  
9

10  
11  
12                   Constantin M. Zohner<sup>1\*</sup>, Leila Mirzagholi<sup>1</sup>, Susanne S. Renner<sup>2</sup>, Lidong Mo<sup>1</sup>, Raymo Bucher<sup>1</sup>, Daniel  
13                   Palouš<sup>1,3</sup>, Yann Vittasse<sup>4</sup>, Yongshuo H. Fu<sup>5</sup>, Benjamin D. Stocker<sup>6</sup>, Thomas W. Crowther<sup>1</sup>  
14

15  
16                   <sup>1</sup>Institute of Integrative Biology, ETH Zurich (Swiss Federal Institute of Technology), Universitätsstrasse 16,  
17                   8092 Zurich, Switzerland; <sup>2</sup>Department of Biology, Washington University, Saint Louis, MO 63130, United  
18                   States; <sup>3</sup>Department of Experimental Plant Biology, Charles University in Prague, Viničná 5, CZ 128 44,  
19                   Czech Republic; <sup>4</sup>WSL Swiss Federal Institute for Forest, Snow and Landscape Research, Birmensdorf,  
20                   Switzerland; <sup>5</sup>College of Water Sciences, Beijing Normal University, Beijing, China; <sup>6</sup>Department of  
21                   Environmental Systems Science, Institute of Agricultural Sciences, ETH Zurich, Switzerland.  
22  
23

24                   \*Author for correspondence: Constantin Zohner, [constantin.zohner@gmail.com](mailto:constantin.zohner@gmail.com)  
25  
26  
27  
28  
29

30                   **This PDF file includes Figures S1–S18**  
31

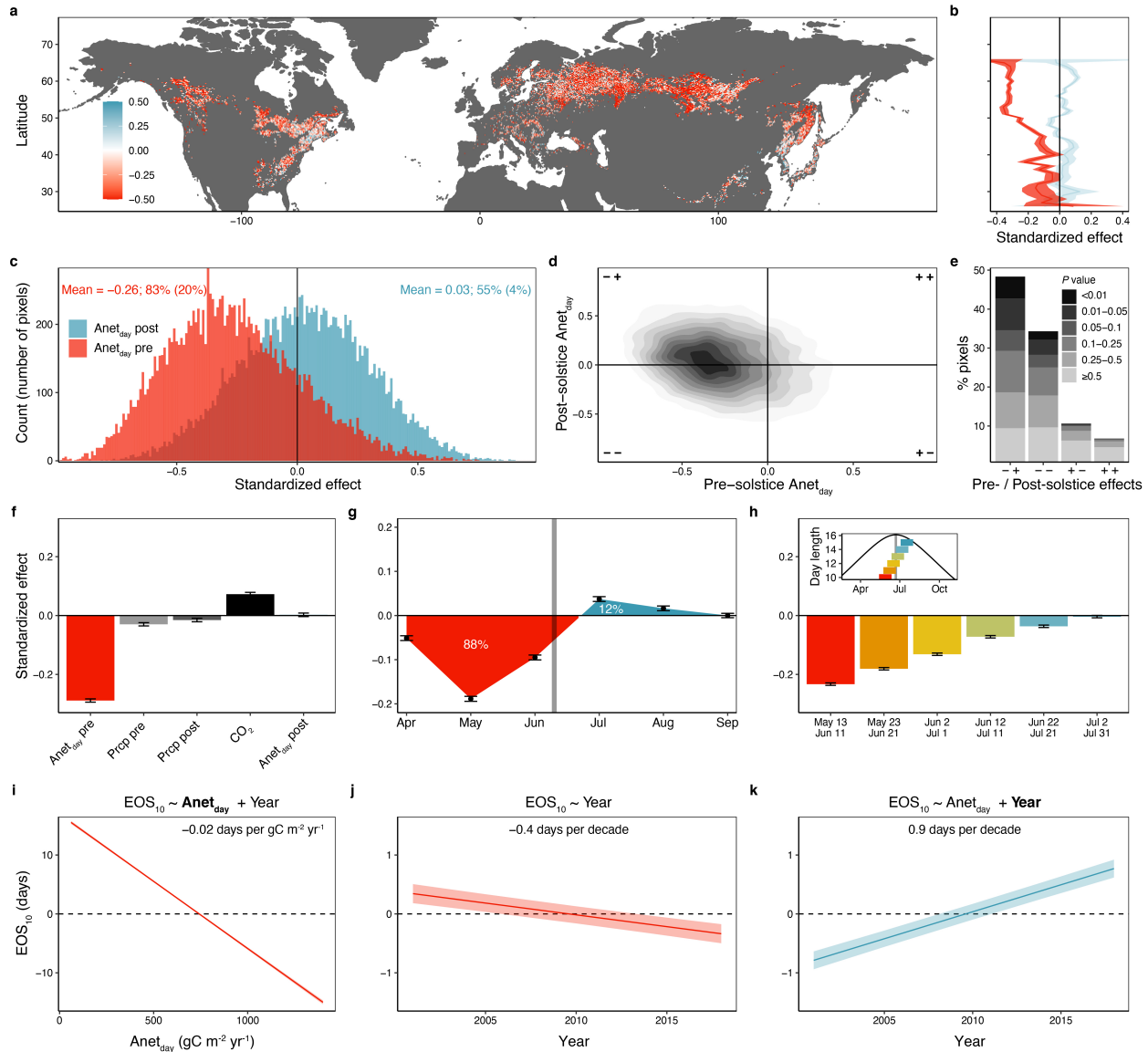


**Fig. S1. Satellite observations reveal consistent advances in the onset of senescence (EOS10) across northern forests in response to enhanced pre-solstice vegetation activity (same as Fig. 2 but using LPJ model-derived net day-time productivity [ $Anet_{day}$ ] as predictor variable).** **a**, Map showing the standardized effects of pre-solstice (March 20 to solstice) productivity ( $Anet_{day}$ ) on EOS<sub>10</sub> timing at 0.25° resolution from linear models, including pre-solstice  $Anet_{day}$  and post-solstice (solstice to mean senescence)  $Anet_{day}$  as predictor variables. Red pixels indicate an earlier EOS<sub>10</sub> under enhanced pre-solstice  $Anet_{day}$ , blue pixels indicate a delayed EOS<sub>10</sub>. **b**, Effect size means and 95% confidence ranges summarized for each degree latitude (pre-solstice effects in red, post-solstice effects in blue). **c**, The distribution of the pre-solstice and post-solstice  $Anet_{day}$  effects across all pixels. Mean pre- and post-solstice  $Anet_{day}$  effect sizes and the percentage of pixels with an advancing pre-solstice  $Anet_{day}$  effect or delaying post-solstice  $Anet_{day}$  effect shown as red and blue text, respectively (percentage of significant pixels at  $P < 0.05$  in brackets). **d**, Two-dimensional density plot of pre- and post-solstice  $Anet_{day}$  effects. Grey scale indicates significance levels of pre-solstice  $Anet_{day}$  effects. **e**, Barplot summarizing the effect direction across all analysed pixels. Grey scale indicates significance levels of pre-solstice  $Anet_{day}$  effects. **f**, The effects of pre-solstice and post-solstice  $Anet_{day}$ , pre-solstice (March 20 to solstice) and post-solstice precipitation (prcp), and atmospheric CO<sub>2</sub>. **g**, Relationship between monthly  $Anet_{day}$  and EOS<sub>10</sub> dates. Percentages reflect the total positive and negative areas under the curve, i.e., the relative negative versus positive effects of seasonal  $Anet_{day}$ . **h**, The univariate effects of one-month-long  $Anet_{day}$  intervals around the summer solstice (May 13 to June 11, May 23 to June 21, June 2 to July 1, June 12 to July 11, June 22 to July 21, and July 2 to July 31; see inset). Analyses in f-h show effect size means and 95% confidence ranges from pixel-level linear models with both predictor and dependent variables standardized. **i-j**, Mean effects ( $\pm 95\%$  confidence ranges) of pre-solstice  $Anet_{day}$  and year on EOS<sub>10</sub> anomalies from mixed effects models where pixels are treated as grouping variables of random intercepts. **i**, Partial effect of pre-solstice  $Anet_{day}$  on EOS<sub>10</sub> anomalies, including both pre-solstice  $Anet_{day}$  and year as fixed effects. **j**, Temporal trend in EOS<sub>10</sub> anomalies with year as single fixed effect. **k**, Partial effect of year on EOS<sub>10</sub> anomalies, where both pre-solstice  $Anet_{day}$  and year are treated as fixed effects.

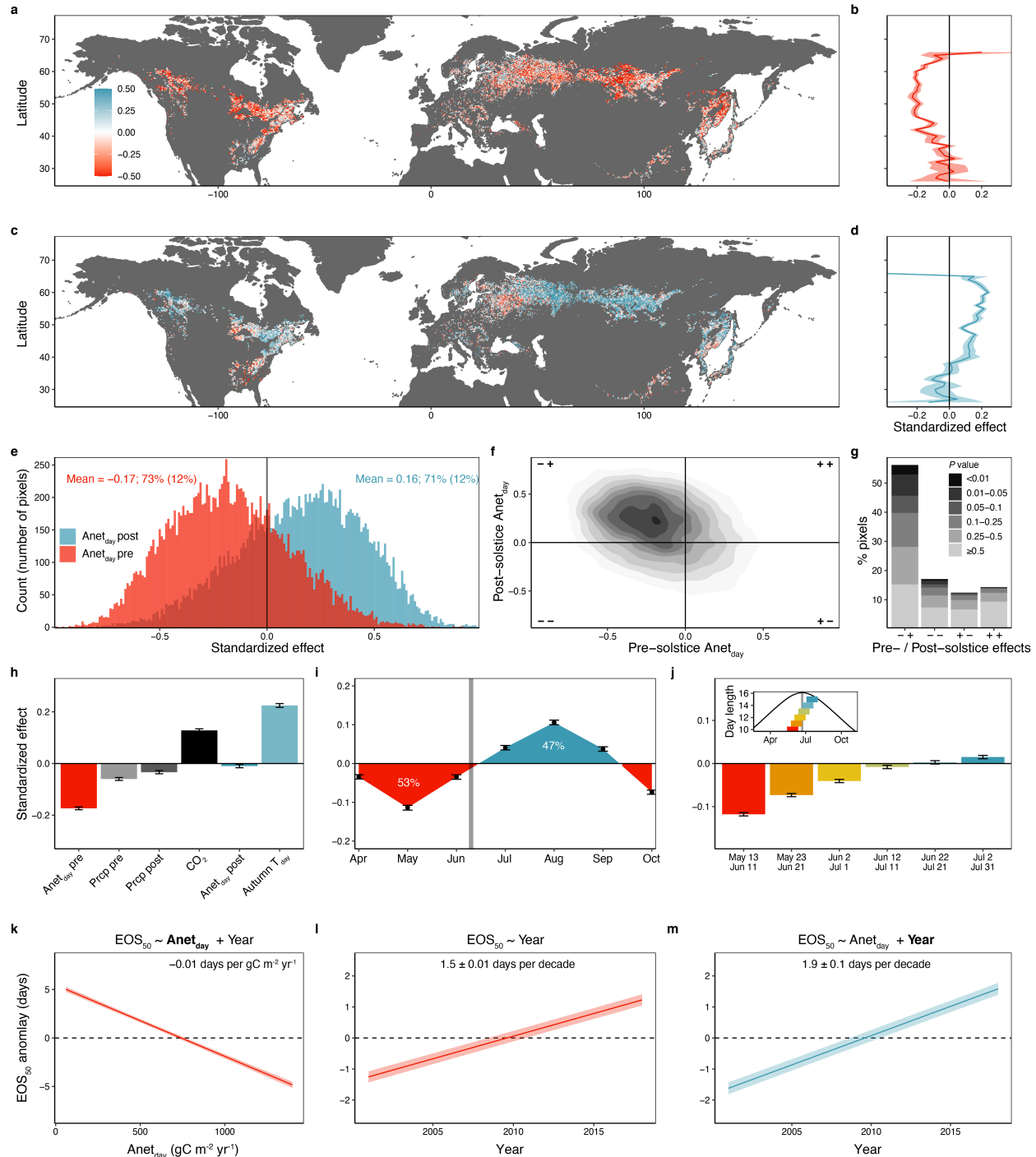


**Fig. S2. The seasonal effects of net daytime photosynthesis ( $Anet_{day}$ ; LPJ model) on inter-annual variations in mid-senescence ( $EOS_{50}$  dates).** **a, c**, Maps showing the standardized effects of pre-solstice  $Anet_{day}$  (leaf-out to solstice; **a**) and post-solstice  $Anet_{day}$  (solstice to mean  $EOS_{50}$ ; **c**) on  $EOS_{50}$  timing at 0.25° resolution from linear models, including pre-solstice  $Anet_{day}$  and post-solstice  $Anet_{day}$  as predictor variables. Red pixels indicate an earlier  $EOS_{50}$  under higher pre-solstice or post-solstice  $Anet_{day}$ , respectively, blue pixels indicate a delayed  $EOS_{50}$ . **b, d**, Effect size means and 95% confidence ranges summarized for each degree latitude (pre-solstice effects in red (**b**), post-solstice effects in blue (**d**)). **e**, The distribution of the pre-solstice and post-solstice  $Anet_{day}$  effects across all pixels. Mean pre- and post-solstice  $Anet_{day}$  effect sizes and the percentage of pixels with a negative pre-solstice  $Anet_{day}$  or positive post-solstice  $Anet_{day}$  effect (percentage of significant pixels at  $P < 0.05$  in brackets) shown as red and blue text, respectively. **f**, Two-dimensional density plot of pre- and post-solstice  $Anet_{day}$  effects. **g**, Barplot summarizing the effect direction across all analysed pixels. Grey scale indicates significance levels of pre-solstice  $Anet_{day}$  effects. **h**, The effects of pre-solstice and post-

54  
55  
56  
57  
58  
59  
60  
61  
62  
63  
64  
65

66 solstice Anet<sub>day</sub>, pre-solstice (March 20 to solstice) and post-solstice precipitation, atmospheric CO<sub>2</sub>, and autumn T<sub>day</sub>. **i**, Relationship  
67 between monthly Anet<sub>day</sub> and EOS<sub>50</sub> dates. Percentages reflect the total positive and negative areas under the curve, i.e., the relative  
68 advancing versus delaying effects of seasonal Anet<sub>day</sub>. **j**, The effects of one-month-long Anet<sub>day</sub> intervals around the summer solstice  
69 (May 13 to June 11, May 23 to June 21, June 2 to July 1, June 12 to July 11, June 22 to July 21, and July 2 to July 31; see inset),  
70 including the respective photosynthesis interval and autumn day-time temperature (Autumn T<sub>day</sub>) as fixed effects. Analyses in **h–j** show  
71 effect size means and 95% confidence ranges from pixel-level linear models with both predictor and dependent variables standardized.  
72 **k–m**, Mean effects ( $\pm 95\%$  confidence ranges) of pre-solstice Anet<sub>day</sub> and year on EOS<sub>50</sub> anomalies from mixed effects models where  
73 pixels are treated as grouping variables of random intercepts. **k**, Partial effect of pre-solstice Anet<sub>day</sub>, including both pre-solstice Anet<sub>day</sub>  
74 and year as fixed effects. **l**, Temporal trend in EOS<sub>50</sub> anomalies with year as single fixed effect. **m**, Partial effect of year, where both  
75 pre-solstice Anet<sub>day</sub> and year are treated as fixed effects.  
76

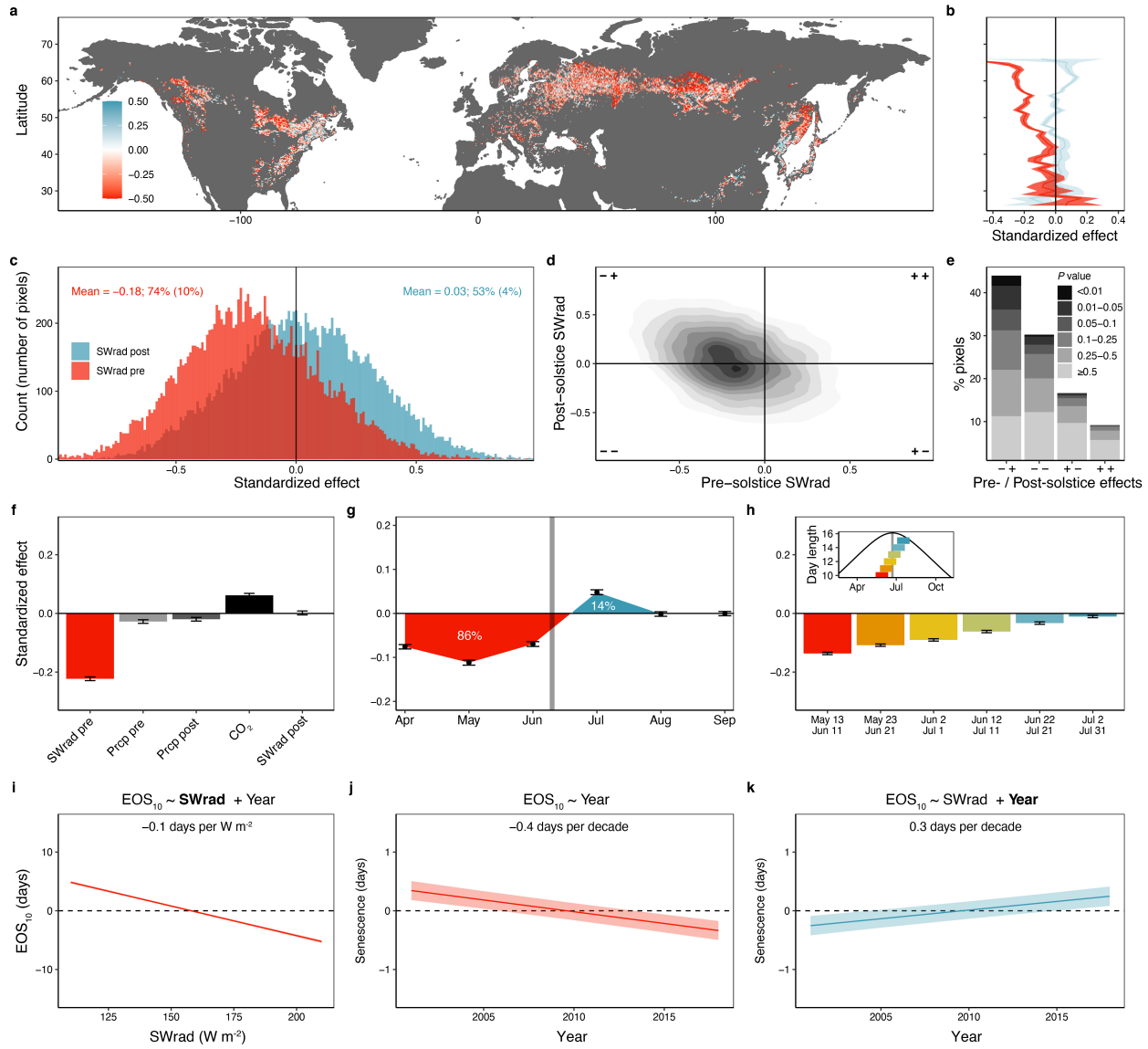


**Fig. S3. The seasonal effects of short-wave radiation (SWrad) on inter-annual variation in senescence onset (EOS<sub>10</sub> dates) [same as Fig. 2 but using cumulative SWrad as predictor variable].** **a**, Map showing the standardized effects of pre-solstice (March 20 to solstice) SWrad on EOS<sub>10</sub> timing at 0.25° resolution from linear models, including pre-solstice SWrad and post-solstice (solstice to mean senescence) SWrad as predictor variables. Red pixels indicate an earlier EOS<sub>10</sub> under enhanced pre-solstice SWrad, blue pixels indicate a delayed EOS<sub>10</sub>. **b**, Effect size means and 95% confidence ranges summarized for each degree latitude (pre-solstice effects in red, post-solstice effects in blue). **c**, The distribution of the pre-solstice and post-solstice SWrad effects across all pixels. Mean pre- and post-solstice SWrad effect sizes and the percentage of pixels with a negative pre-solstice SWrad or positive post-solstice SWrad effect (percentage of significant pixels at  $P < 0.05$  in brackets) shown as red and blue text, respectively. **d**, Two-dimensional density plot of pre- and post-solstice SWrad effects. **e**, Barplot summarizing the effect direction across all analysed pixels. Grey scale indicates significance levels of pre-solstice SWrad effects. **f**, The effects of pre-solstice and post-solstice SWrad and precipitation and atmospheric CO<sub>2</sub>. **g**, Relationship between monthly SWrad and EOS<sub>10</sub> dates. Percentages reflect the total positive and negative areas under the curve, i.e., the relative advancing versus delaying effects of seasonal SWrad. **h**, The univariate effects of one-month-long SWrad intervals around the summer solstice (May 13 to June 11, May 23 to June 21, June 2 to July 1, June 12 to July 11, June 22 to July 21, and July 2 to July 31; see inset). Analyses in **f-h** show effect size means and 95% confidence ranges from pixel-level linear models with both predictor and dependent variables standardized. **i-k**, Mean effects ( $\pm 95\%$  confidence ranges) of pre-solstice SWrad and year on EOS<sub>10</sub> anomalies from mixed effects models where pixels are treated as grouping variables of random intercepts. **i**, Partial effect of pre-solstice SWrad, including both pre-solstice SWrad and year as fixed effects. **j**, Temporal trend in EOS<sub>10</sub> anomalies with year as single fixed effect. **k**, Partial effect of year, where both pre-solstice SWrad and year are treated as fixed effects.

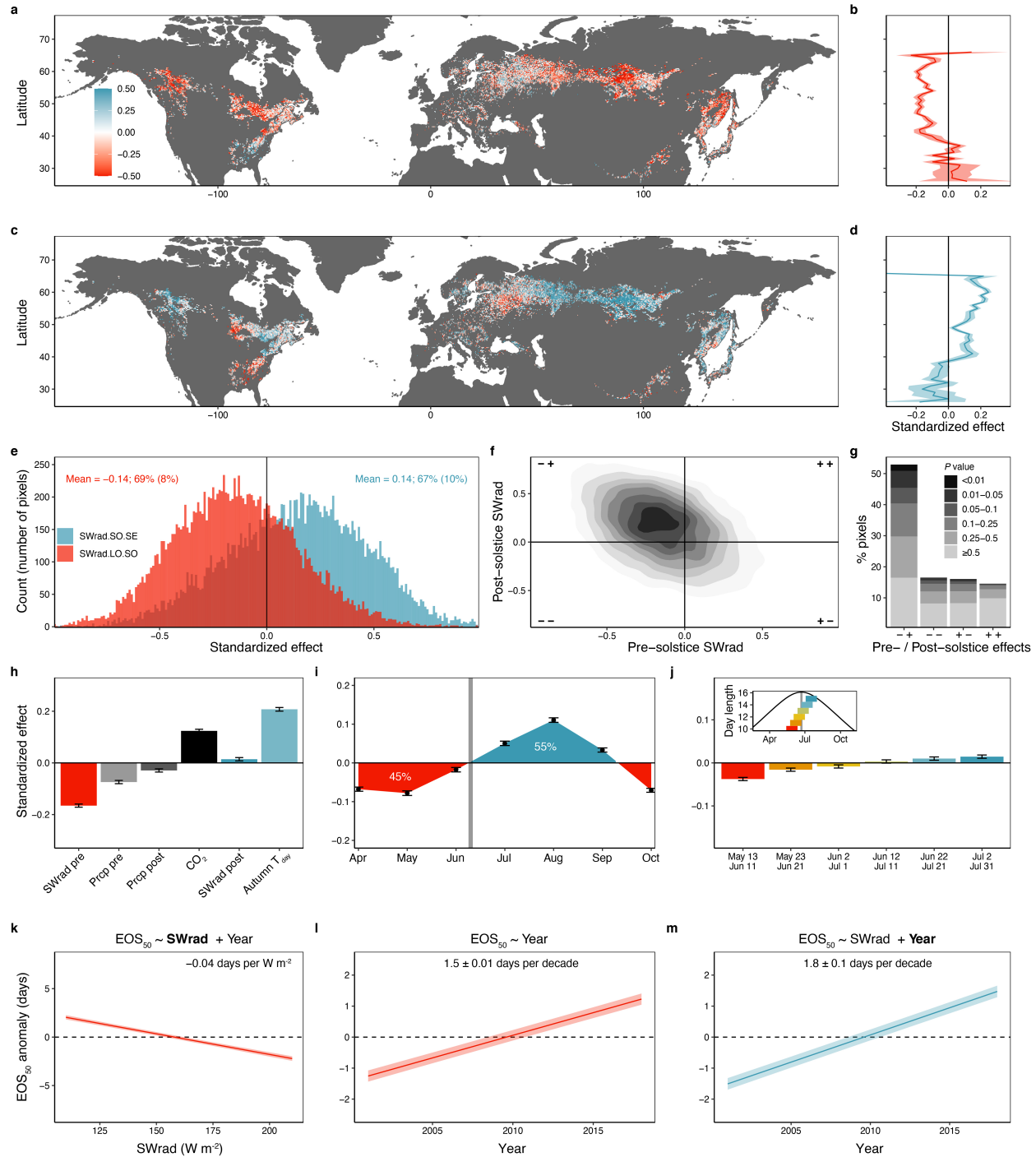


**Fig. S4. The seasonal effects of cumulative SWrad on inter-annual variation in mid-senescence (EOS<sub>50</sub> dates).** **a, c**, Maps showing the standardized effects of pre-solstice SWrad (March 20 to solstice; **a**) and post-solstice SWrad (solstice to mean EOS<sub>50</sub>; **c**) on EOS<sub>50</sub> timing at 0.25° resolution from linear models, including pre-solstice SWrad and post-solstice SWrad as predictor variables. Red pixels indicate an earlier EOS<sub>50</sub> under higher pre-solstice or post-solstice SWrad, respectively, blue pixels indicate a delayed EOS<sub>50</sub>. **b, d**, Effect size means and 95% confidence ranges summarized for each degree latitude (pre-solstice effects in red (**b**)), post-solstice effects in blue (**d**)). **e**, The distribution of the pre-solstice and post-solstice SWrad effects across all pixels. Mean pre- and post-solstice SWrad effect sizes and the percentage of pixels with a negative pre-solstice SWrad or positive post-solstice SWrad effect (percentage of significant pixels at  $P < 0.05$  in brackets) shown as red and blue text, respectively. **f**, Two-dimensional density plot of pre- and post-solstice SWrad effects. **g**, Barplot summarizing the effect direction across all analysed pixels. Grey scale indicates significance levels of pre-solstice SWrad effects. **h**, The effects of pre-solstice and post-solstice SWrad and precipitation, atmospheric CO<sub>2</sub>, and autumn day-time temperature ( $T_{day}$ ). **i**, Relationship between monthly SWrad and EOS<sub>50</sub> dates. Percentages reflect the total

positive and negative areas under the curve, i.e., the relative advancing versus delaying effects of seasonal SWrad. **j**, The effects of one-month-long SWrad intervals around the summer solstice (May 13 to June 11, May 23 to June 21, June 2 to July 1, June 12 to July 11, June 22 to July 21, and July 2 to July 31; see inset), including the respective SWrad interval and autumn day-time temperature (Autumn  $T_{day}$ ) as fixed effects. Analyses in **h–j** show effect size means and 95% confidence ranges from pixel-level linear models with both predictor and dependent variables standardized. **k–m**, Mean effects ( $\pm 95\%$  confidence ranges) of pre-solstice SWrad and year on  $EOS_{50}$  anomalies from mixed effects models where pixels are treated as grouping variables of random intercepts. **k**, Partial effect of pre-solstice SWrad, including both pre-solstice SWrad and year as fixed effects. **l**, Temporal trend in  $EOS_{50}$  anomalies with year as single fixed effect. **m**, Partial effect of year, where both pre-solstice SWrad and year are treated as fixed effects.

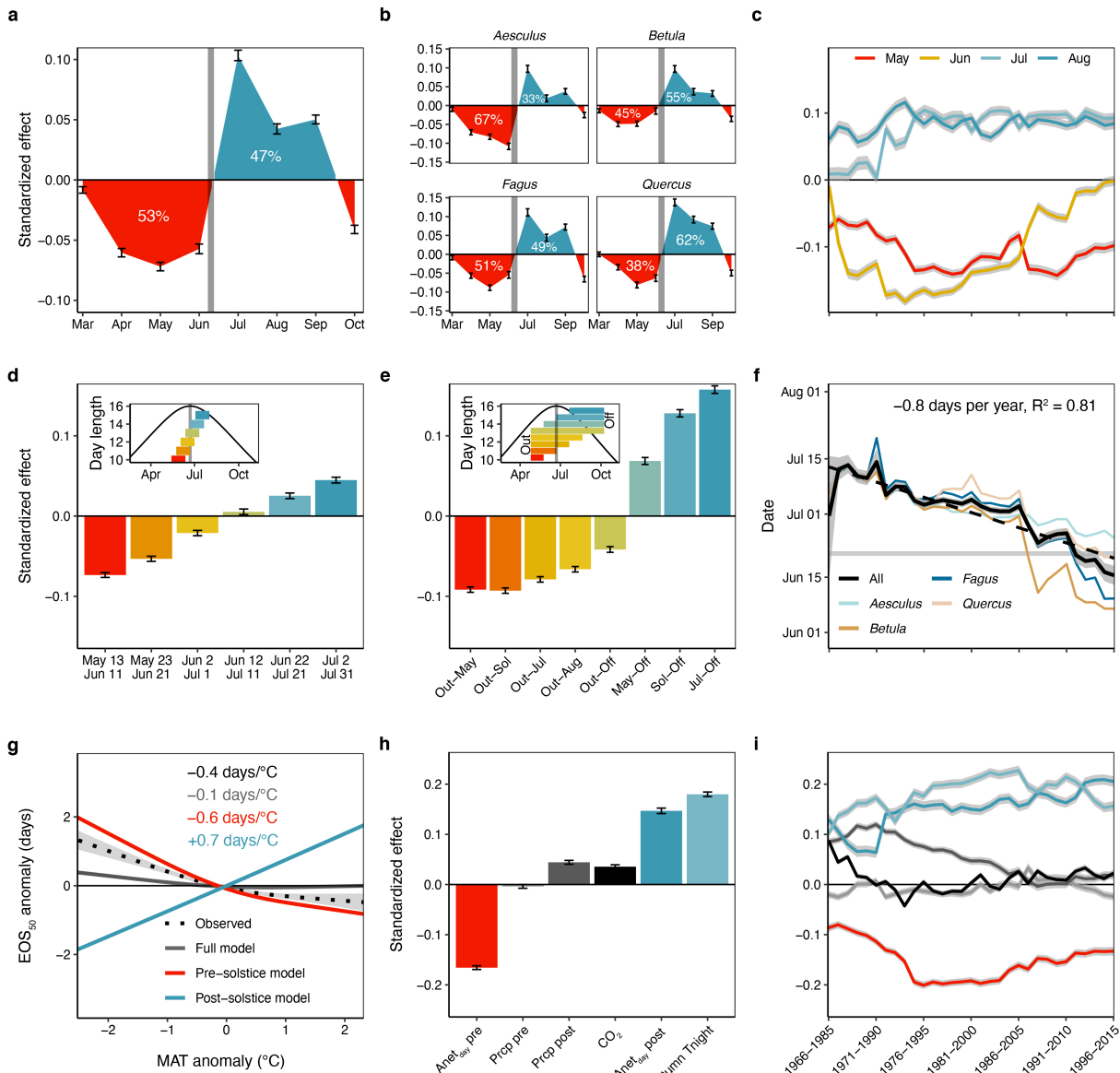


**Fig. S5. The seasonal effects of photosynthesis on inter-annual variation in mid-senescence (EOS<sub>50</sub> dates) from European long-term observations (PEP725 data; same as Fig. 3 but using the P model<sup>23</sup> to estimate daily photosynthesis).** **a**, Effects of monthly (March to October) photosynthesis on autumn senescence dates. Percentages reflect the total positive and negative areas under the curve, i.e., the relative advancing versus delaying effects of seasonal photosynthesis. **b**, Species-level results. **c**, Moving window analysis, showing the effects of May (leaf-out to 31 May), June, July, and August/September (1 August to 30 September) photosynthesis for each 20-year time period from 1966 to 2015. **d**, The effects of one-month-long photosynthesis intervals around the summer solstice (May 13 to June 11, May 23 to June 21, June 2 to July 1, June 12 to July 11, June 22 to July 21, and July 2 to July 31; see inset), including the respective photosynthesis interval and autumn night-time temperature (Autumn T<sub>night</sub>) as fixed effects. **e**, The effects of cumulative photosynthesis from leaf-out to May 22 (Out–May), leaf-out to solstice (Out–Sol), leaf-out to July 21 (Out–Jul), leaf-out to August 20 (Out–Aug), leaf-out to mean senescence (Out–Off), May 22 to mean senescence (May–Off), solstice to mean senescence (Sol–Off), and July 21 to mean senescence (Jul–Off), including the respective photosynthesis interval as single fixed effect. **f**, Moving-window analysis, showing the ‘reversal’ dates when the photosynthesis effect switches from negative to positive for each 20-year time period from 1966 to 2015 (based on monthly correlations, see panels **a–c**). On average, the reversal date advanced by 0.8 days per year. **g–i**, The effects of pre-solstice (leaf-out to solstice) and post-solstice (solstice to mean senescence) photosynthesis, pre-solstice (March 20 to solstice) and post-solstice precipitation, atmospheric CO<sub>2</sub>, and Autumn T<sub>night</sub>. **g**, Model predictions in response to mean annual temperature (MAT) anomalies (black dashed line: observed trend; black solid line: full model prediction; red line: model prediction including only pre-solstice photosynthesis and precipitation and CO<sub>2</sub> as predictors; blue line: model prediction including only post-solstice photosynthesis and precipitation, CO<sub>2</sub>, and Autumn T<sub>night</sub>). **h**, Standardised effects. **i**, 20-year moving-window analysis of the effects (colours as in panel **h**). Analyses show effect size means  $\pm$  2 s.e. from linear mixed models, including time series and species (**a,c–i**) or only time series (**b,f**) as random effects, with both predictor and dependent variables standardized.

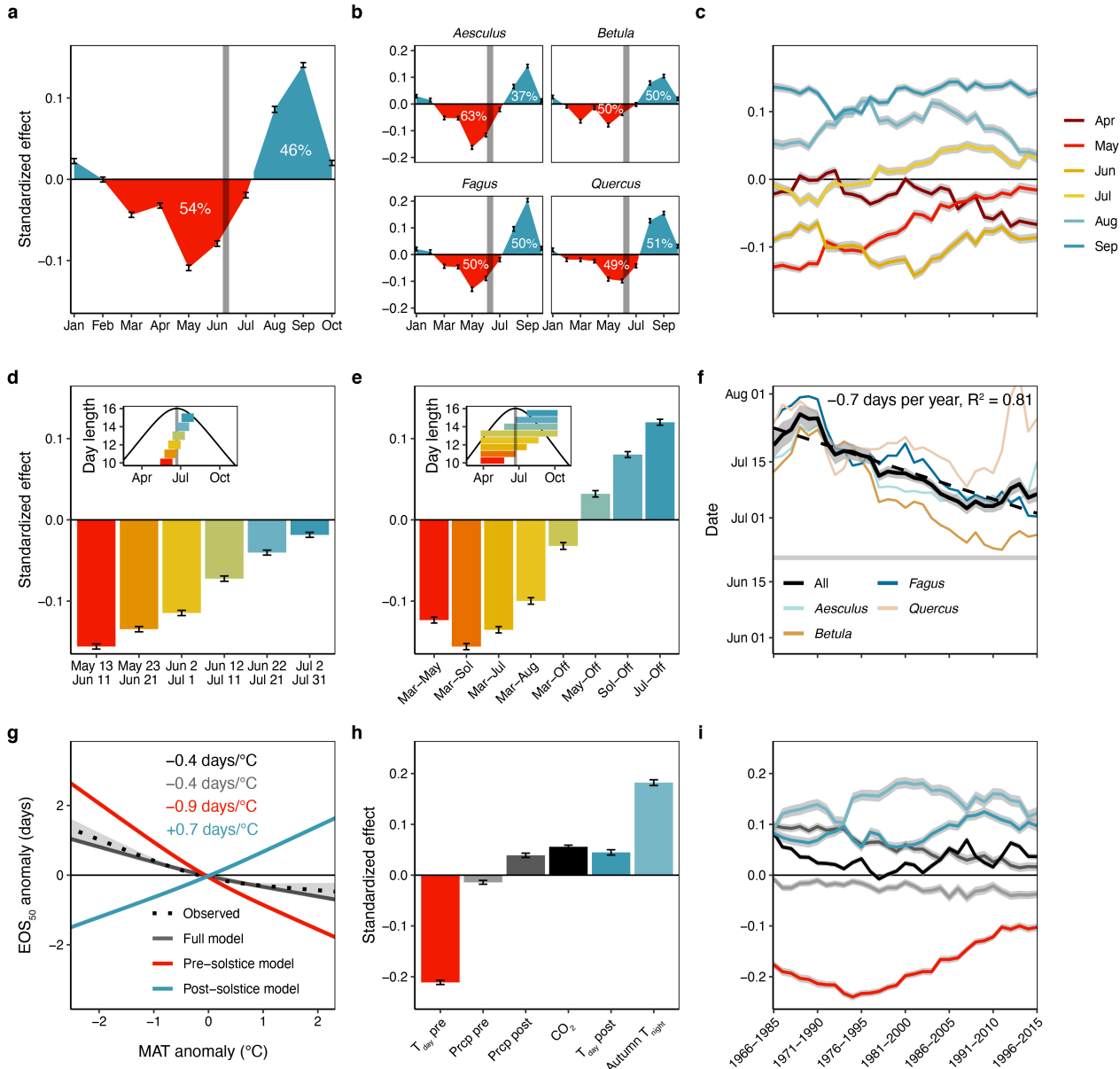
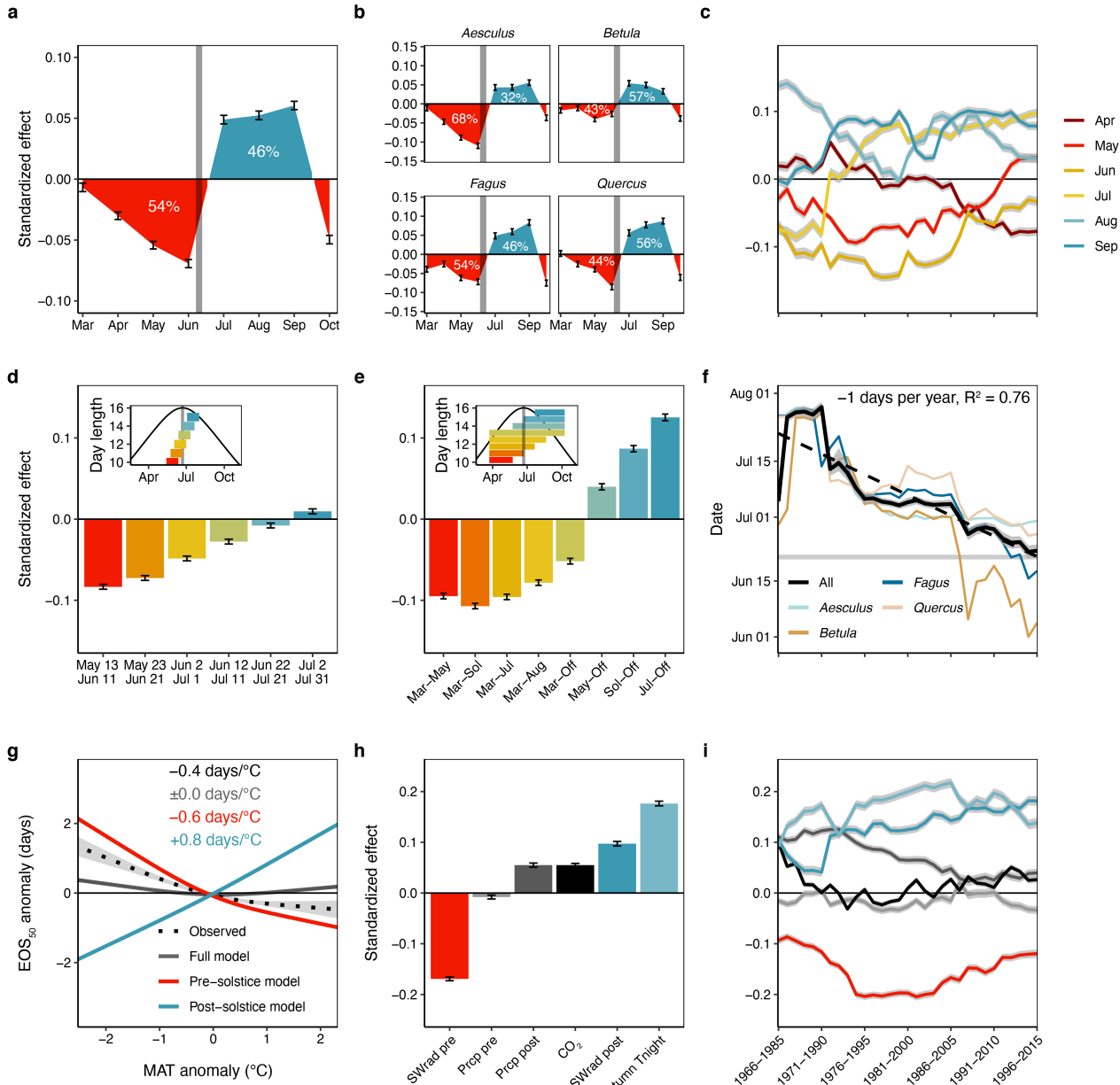


**Fig. S6. The seasonal effects of temperature on inter-annual variation in mid-senescence (EOS<sub>50</sub> dates) from European long-term observations (PEP725 data; same as Fig. 3 but using day-time temperature [ $T_{\text{day}}$ ] as predictor variable). a, Effects of monthly (January to October) day-time temperature on autumn senescence dates. Percentages reflect the total positive and negative areas under the curve, i.e., the relative advancing versus delaying effects of temperature. b, Species-level results. c, Moving window analysis, showing the effects of monthly (April to September) temperature for each 20-year time period from 1966 to 2015. d, The effects of one-month-long temperature intervals around the summer solstice (May 13 to June 11, May 23 to June 21, June 2 to July 1, June 12 to July 11, June 22 to July 21, and July 2 to July 31; see inset), including the respective temperature interval and autumn night-time temperature (Autumn  $T_{\text{night}}$ ) as fixed effects. e, The effects of mean temperature from March 20 to May 22 (March–May), March 20 to solstice (March–Sol), March 20 to July 21 (March–Jul), March 20 to August 20 (March–Aug), March 20 to mean senescence (March–Off), May 22 to mean senescence (May–Off), solstice to mean senescence (Sol–Off), and July 21 to mean senescence (Jul–Off), including the respective temperature interval as single fixed effect. f, Moving-window analysis, showing the ‘reversal’ dates when the air temperature effect switches from negative to positive for each 20-year time period from 1966 to 2015 (based on monthly correlations, see panels a–c). On average, the reversal date advanced by 0.7 days per year. g–i, Effects of pre-solstice ( $T_{\text{day pre}}$ ; March 20 to solstice) and post-solstice temperature ( $T_{\text{day post}}$ ; solstice to mean senescence), pre-solstice and post-solstice precipitation (Prop pre/post), atmospheric  $\text{CO}_2$ , and Autumn  $T_{\text{night}}$ . g, Model predictions in response to mean annual temperature (MAT) anomalies (black dashed line: observed trend; black solid line: full model prediction; red line: model prediction including only pre-solstice temperature and precipitation and  $\text{CO}_2$  as predictors; blue line: model prediction including only post-solstice temperature and precipitation,  $\text{CO}_2$ , and Autumn  $T_{\text{night}}$ ). h, Standardised effects. i, 20-year moving-window analysis of the effects (colours as in panel h). Analyses show effect size means  $\pm 2$  s.e. from linear mixed models, including time series and species (a,c–i) or only time series (b,f) as random effects, with both predictor and dependent variables standardized.**

144  
145  
146  
147  
148  
149  
150  
151  
152  
153  
154  
155  
156  
157  
158  
159  
160  
161  
162  
163  
164  
165



166  
167 **Fig. S7. The seasonal effects of radiation on inter-annual variation in mid-senescence (EOS<sub>50</sub> dates) from European long-term**  
168 **observations (PEP725 data; same as Fig. 3 but using cumulative short-wave radiation [SWrad] as predictor variable).** a, Effects  
169 of monthly (March to October) SWrad values on autumn senescence dates. Percentages reflect the total positive and negative areas  
170 under the curve, i.e., the relative advancing versus delaying effects of SWrad. b, Species-level results. c, Moving-window analysis,  
171 showing the effects monthly (April to September) SWrad for each 20-year time period from 1966 to 2015. d, Effects of one-month-long  
172 SWrad intervals around the summer solstice (May 13 to June 11, May 23 to June 21, June 2 to July 1, June 12 to July 11, June 22 to  
173 July 21, and July 2 to July 31; see inset), including the respective SWrad interval and autumn night-time temperature (Autumn T<sub>night</sub>)  
174 as fixed effects. e, Effects of cumulative SWrad from March 20 to May 22 (Mar-May), March 20 to solstice (Mar-Sol), March 20 to July  
175 21 (Mar-Jul), March 20 to August 20 (Mar-Aug), March 20 to mean senescence (Mar-Off), May 22 to mean senescence (May-Off),  
176 solstice to mean senescence (Sol-Off), and July 21 to mean senescence (Jul-Off), including the respective SWrad interval as single  
177 fixed effect. f, Moving-window analysis, showing the ‘reversal’ dates when the SWrad effect switches from negative to positive for each  
178 20-year time period from 1966 to 2015 (based on monthly correlations, see panels a–c). On average, the reversal date advanced by  
179 1 day per year. g–i, Effects of pre-solstice (leaf-out to solstice) and post-solstice (solstice to mean senescence) SWrad, pre-solstice  
180 (March 20 to solstice) and post-solstice precipitation, atmospheric CO<sub>2</sub>, and Autumn T<sub>night</sub>. g, Model predictions in response to mean  
181 annual temperature (MAT) anomalies (black dashed line: observed trend; black solid line: full model prediction; red line: model  
182 prediction including only pre-solstice SWrad and precipitation and CO<sub>2</sub> as predictors; blue line: model prediction including only post-  
183 solstice SWrad and precipitation, CO<sub>2</sub>, and Autumn T<sub>night</sub>). h, Standardised effects. i, 20-year moving-window analysis of the effects  
184 (colours as in panel h). Analyses show effect size means ± 2 s.e. from linear mixed models, including time series and species (a,c–i)  
185 or only time series (b,f) as random effects, with both predictor and dependent variables standardized.

186

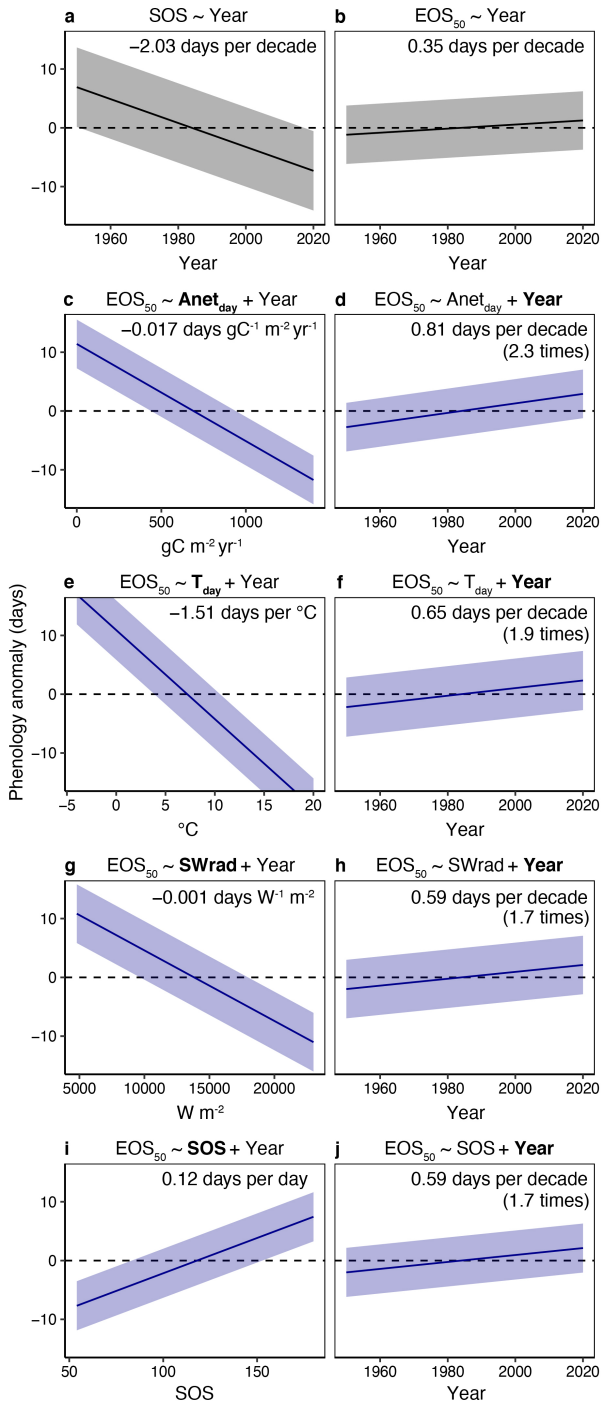
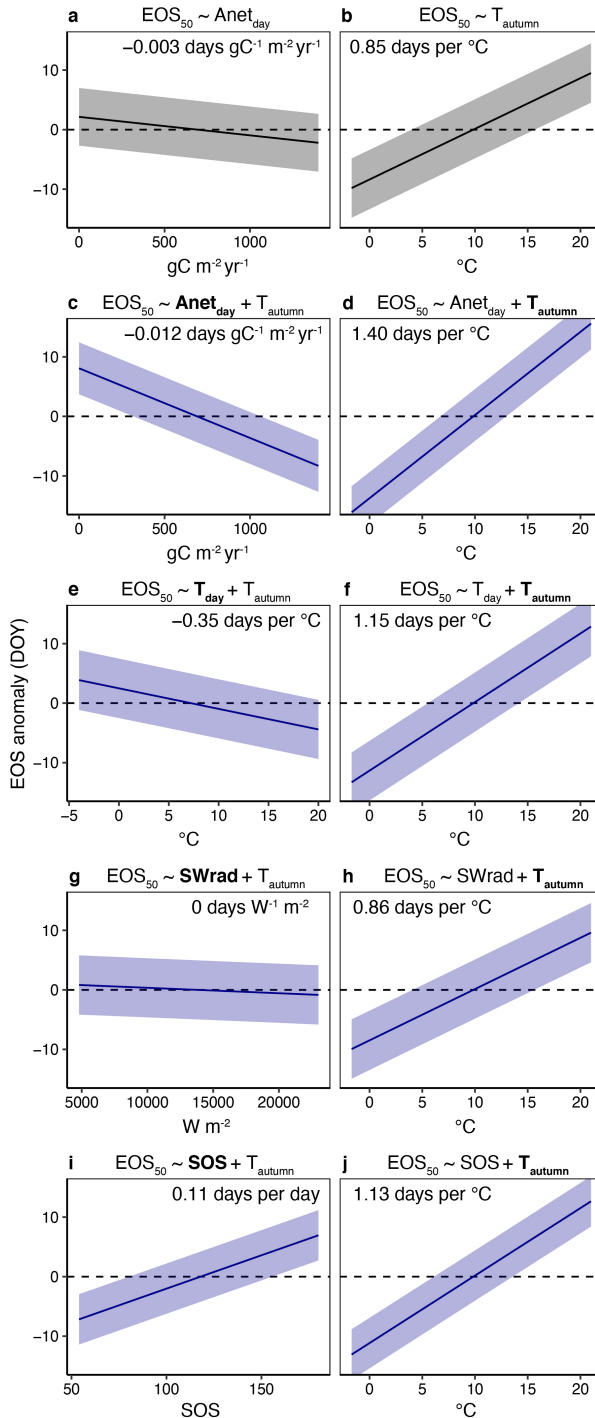


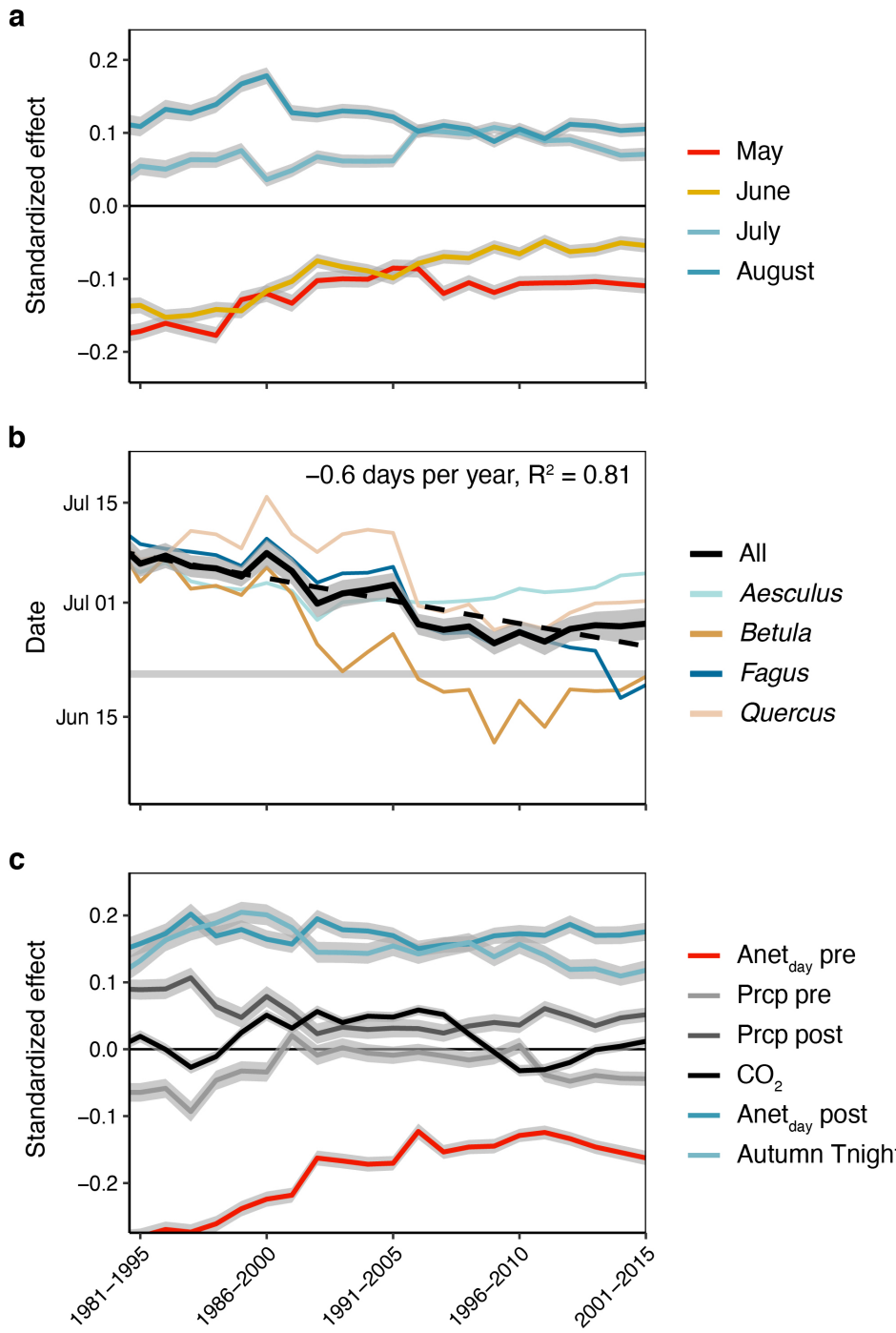
Fig. S8. Temporal relationships among pre-solstice carbon uptake (Anet<sub>day</sub>) or climate, year and phenological dates using the local PEP725 observations. **a, b**, Temporal changes in SOS (**a**) and EOS<sub>50</sub> anomalies (**b**) as inferred from a univariate mixed effects model, including year as fixed effect and time series and species as grouping variables of random intercepts. On average, SOS advanced by  $2.03 \pm 0.02$  days per decade (mean  $\pm$  2 standard errors), EOS<sub>50</sub> delayed by  $0.35 \pm 0.02$  days per decade. **c, d**, Partial effects of pre-solstice Anet<sub>day</sub> (**c**) and year (**d**) on EOS<sub>50</sub> dates, where both pre-solstice Anet<sub>day</sub> and year are treated as fixed effects, and time series and species are treated as grouping variables of random intercepts. Pre-solstice Anet<sub>day</sub> was simulated using the LPJ-GUESS model. Each 100 g m<sup>-2</sup> increase in pre-season carbon uptake results in  $1.7 \pm 0.02$  days earlier EOS<sub>50</sub>. When controlling for this negative effect of pre-solstice Anet<sub>day</sub>, the effect of year on EOS<sub>50</sub> dates increased by 2.3 times to an average delay in EOS<sub>50</sub> of  $0.81 \pm 0.03$  days per decade. **e–j**, Same as panels **c** and **d** but including pre-solstice (March 20 to June 21) day-time temperature T<sub>day</sub> (**e,f**), pre-solstice short-wave radiation (**g,h**), or SOS dates (**i,j**) instead of pre-solstice photosynthesis as fixed effect in addition to year.

187  
188  
189  
190  
191  
192  
193  
194  
195  
196  
197  
198  
199



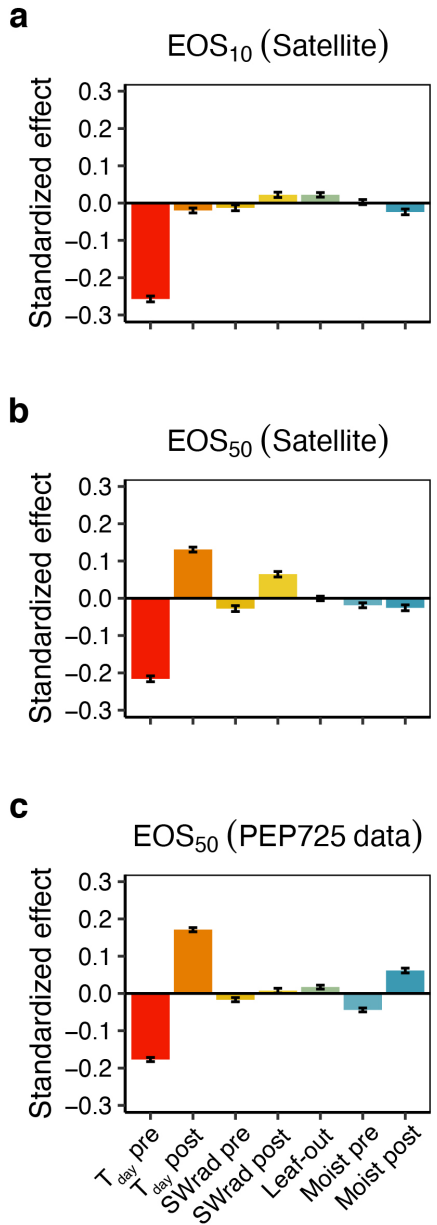
200  
201  
202  
203  
204  
205  
206  
207  
208  
209  
210  
211  
212  
213

**Fig. S9. Spatial relationships among pre-solstice carbon uptake ( $Anet_{day}$ ), September temperature ( $T_{autumn}$ ) and EOS<sub>50</sub> dates using the local PEP725 observations.** **a, b**, Spatial changes in EOS<sub>50</sub> anomalies in response to pre-solstice  $Anet_{day}$  (**a**) and  $T_{autumn}$  (**b**) as inferred from a univariate mixed effects model, including year and species as grouping variables of random intercepts. On average, EOS<sub>50</sub> dates advance by  $0.3 \pm 0.04$  (mean  $\pm$  2 standard errors) days per each  $100 \text{ g m}^{-2}$  increase in pre-season carbon uptake and delay by  $0.85 \pm 0.03$  days per each  $^\circ\text{C}$  increase in  $T_{autumn}$ . **c, d**, Partial effects of pre-solstice  $Anet_{day}$  (**c**) and  $T_{autumn}$  (**d**) on EOS<sub>50</sub> dates, where both pre-solstice photosynthesis and  $T_{autumn}$  are treated as fixed effects, and year and species are treated as grouping variables of random intercepts. Pre-solstice photosynthesis was simulated using the LPJ-GUESS model. Each  $100 \text{ g m}^{-2}$  increase in pre-season carbon uptake results in  $1.17 \pm 0.05$  days earlier EOS<sub>50</sub>. When controlling for this negative effect of pre-solstice photosynthesis, the effect of  $T_{autumn}$  on EOS<sub>50</sub> dates increases by 1.7 times to an average delay in senescence of  $1.40 \pm 0.04$  days per each  $^\circ\text{C}$  increase in  $T_{autumn}$ . **e–j**, Same as panels c and d but including pre-solstice (March 20 to June 21) day-time temperature  $T_{day}$  (**e,f**), pre-solstice short-wave radiation (**g,h**), or SOS dates (**i,j**) instead of pre-solstice  $Anet_{day}$  as fixed effect in addition to  $T_{autumn}$ .

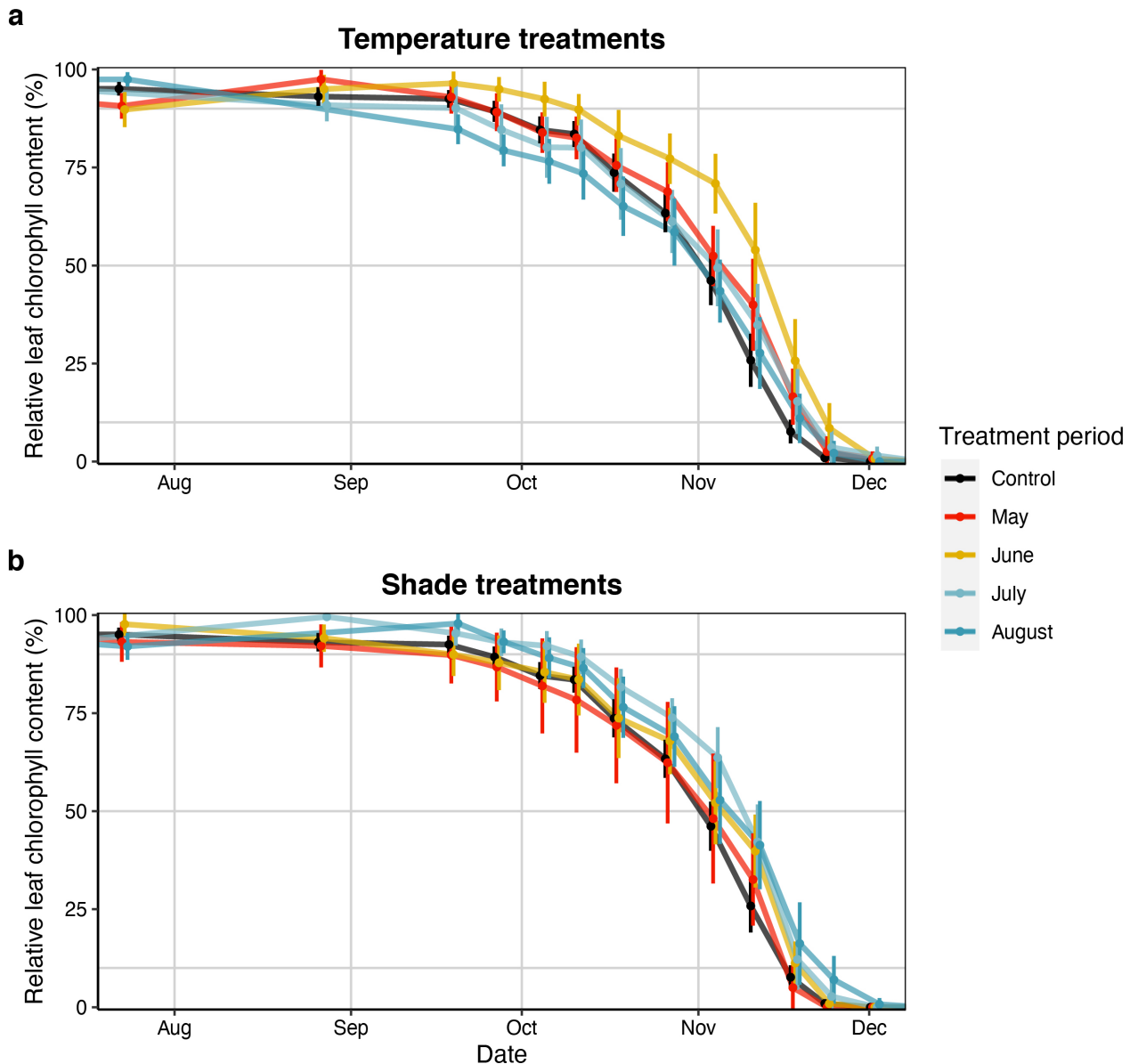


214  
215 **Fig. S10. Same as Fig. 3c, f, i but using 15-year moving window analyses covering the period 1980–**  
216 **2015. a,** The standardized effects of May (leaf-out to 31 May), June, July, and August/September (1 August  
217 to 30 September) photosynthesis. **b,** The ‘reversal’ dates when the photosynthesis effect switches from  
218 negative to positive for each 20-year time period from 1966 to 2015 (based on monthly correlations, see  
219 panels a–c in Fig. 2). On average, the reversal date advanced by 0.6 days per year. **c,** The effects of pre-  
220 solstice (leaf-out to solstice) and post-solstice (solstice to mean senescence) photosynthesis, pre-solstice  
221 (March 20 to solstice) and post-solstice precipitation, atmospheric CO<sub>2</sub>, and autumn night-time temperature  
222 (Autumn T<sub>night</sub>). All analyses are based on linear mixed models, including time series and species as random  
223 effects.

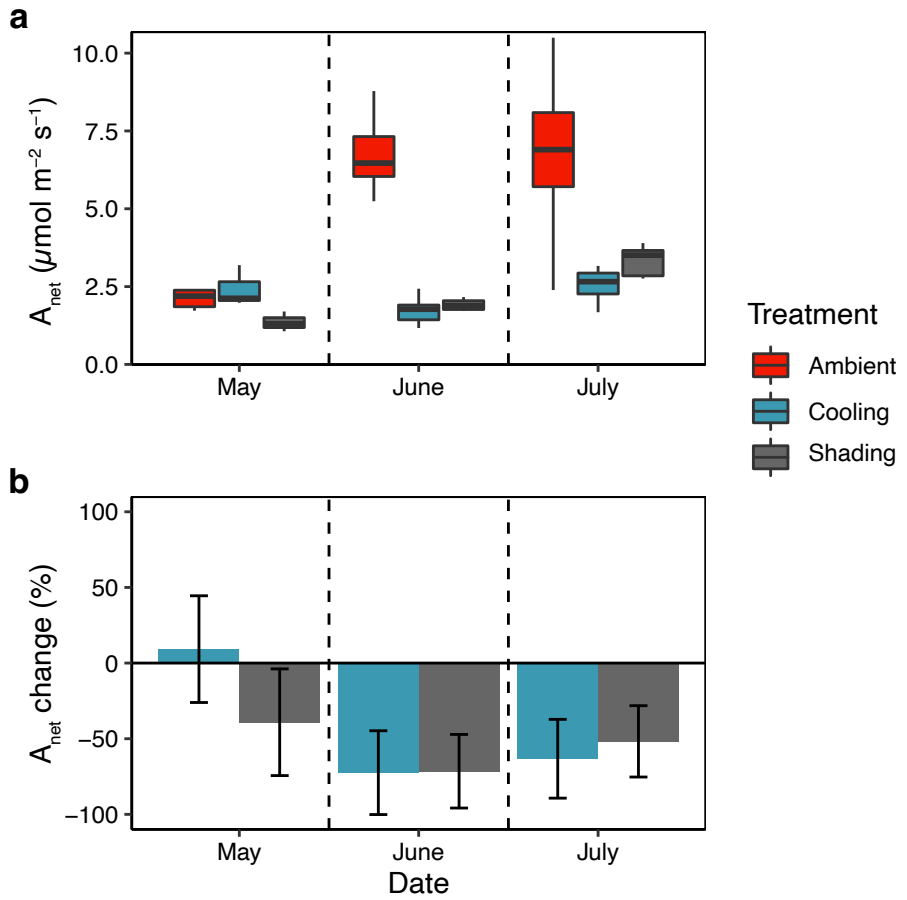
224



225  
226 **Fig. S11. The effects of pre- and post-solstice temperature, radiation, water availability and spring**  
227 **leaf-out dates on inter-annual variation in the timing of EOS<sub>10</sub> (a) and EOS<sub>50</sub> (b, c) [same as Fig. 4 but**  
228 **using soil moisture instead of precipitation to represent water availability].** We ran linear models  
229 including mean day-time temperature ( $T_{\text{day}}$ ), short-wave radiation (SWrad) and soil moisture (moist) from  
230 March 20 to June 21 (pre-solstice) and from June 22 to the mean EOS date of each time series (post-  
231 solstice) as well as spring leaf-out dates as predictor variables. Models were run at the pixel-level (a, b) or  
232 individual-level (c) and the mean effects ( $\pm 95\%$  confidence intervals) are shown. All variables were  
233 standardized to allow for effect size comparison.  
234

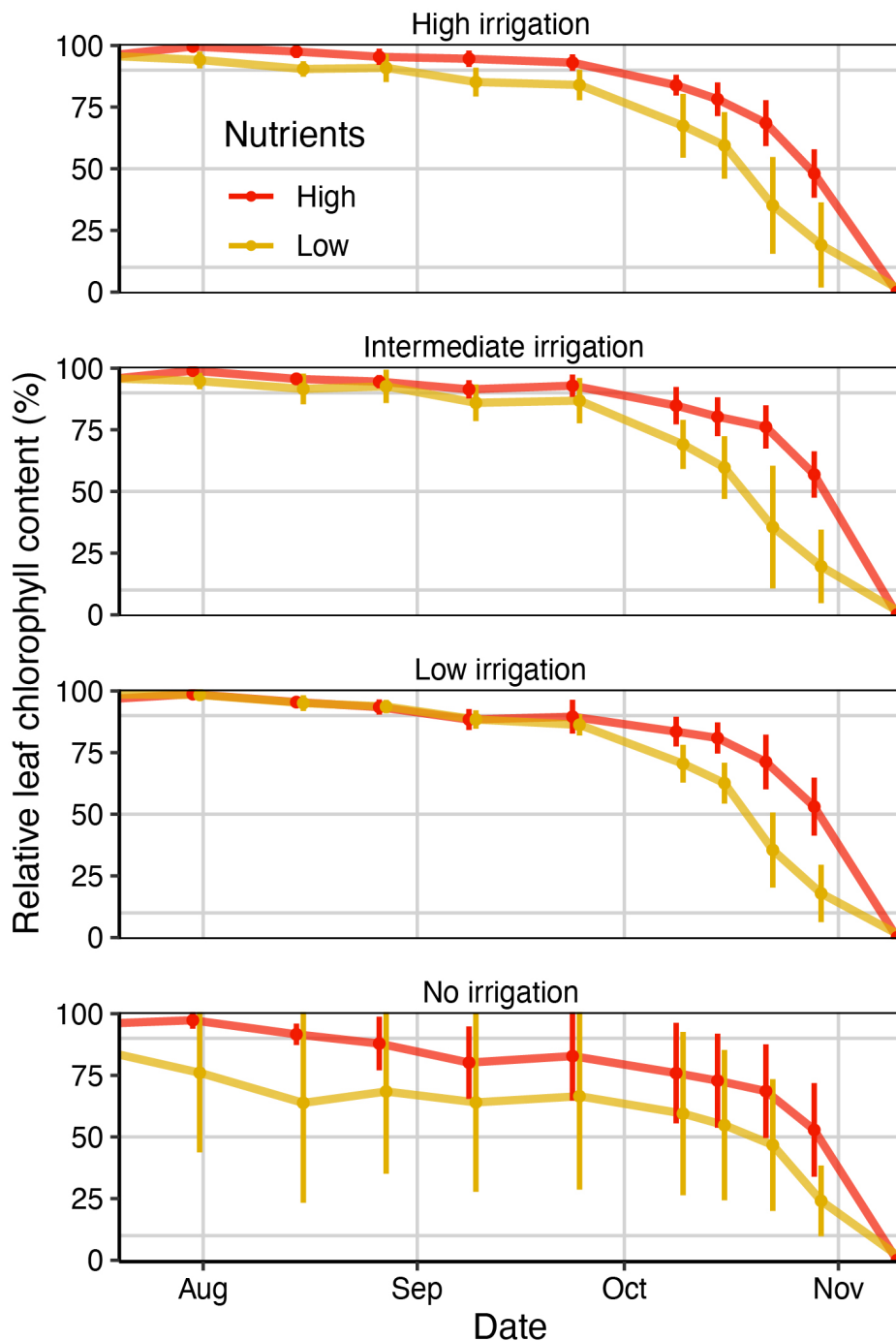


235  
236  
237 **Fig. S12. Autumnal decline in leaf chlorophyll content in response to cooling (a) and shading (b)**  
238 **during May, June, July or August (Experiment 1).** Relative leaf chlorophyll content relative to the  
239 maximum chlorophyll content observed for each tree. The black line represents the control treatment. Error  
240 bars represent means  $\pm$  95% confidence intervals.  
241



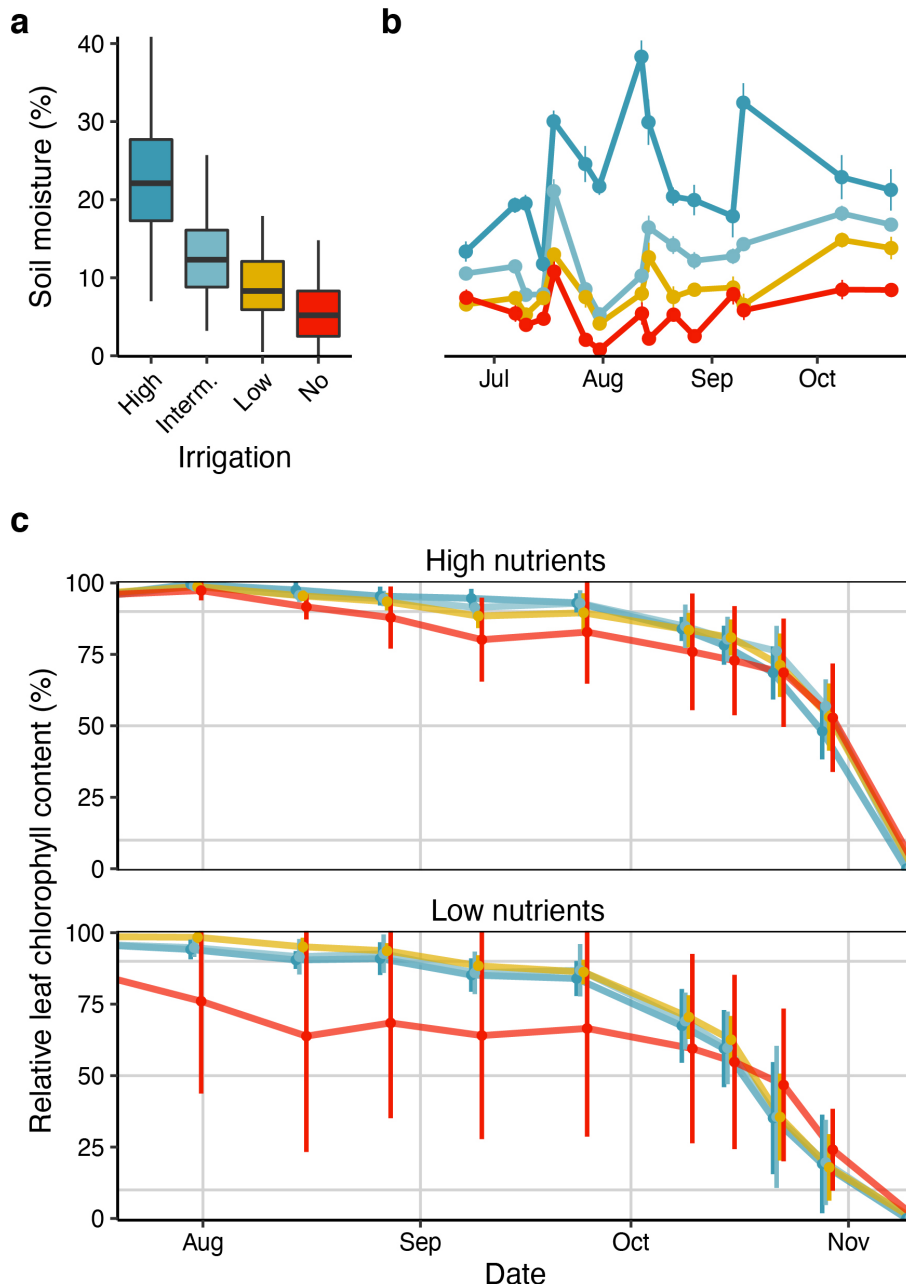
242  
243  
244  
245  
246  
247

**Fig. S13. Photosynthesis rates of *Fagus sylvatica* trees under cooling, shading and ambient conditions from May–July (Experiment 1). a**, Absolute photosynthesis of the cooling, shading and control treatment trees. **b**, Photosynthesis rates of the cooling and shading treatments relative to the control (in %).



248  
 249  
**Fig. S14. Autumnal decline in leaf chlorophyll content under high (red) and low (orange) soil**  
 250 **nutrients (Experiment 2).** Relative leaf chlorophyll content relative to the maximum chlorophyll content  
 251 observed for each tree. Panels show chlorophyll curves under high, intermediate, low, and no irrigation,  
 252 respectively. Error bars represent means  $\pm$  95% confidence intervals.  
 253

254



255  
256 **Fig. S15. Autumnal decline in leaf chlorophyll content in response to a soil moisture gradient**  
257 **(Experiment 2).** **a, b,** Total (a) and seasonal (b) variation in soil moisture levels across the four irrigation  
258 treatments. **c,** Relative leaf chlorophyll content relative to the maximum chlorophyll content observed  
259 for each tree. Upper panel shows chlorophyll curves for the high nutrient, lower panel for the low  
260 nutrient treatments. Error bars represent means  $\pm$  95% confidence intervals.

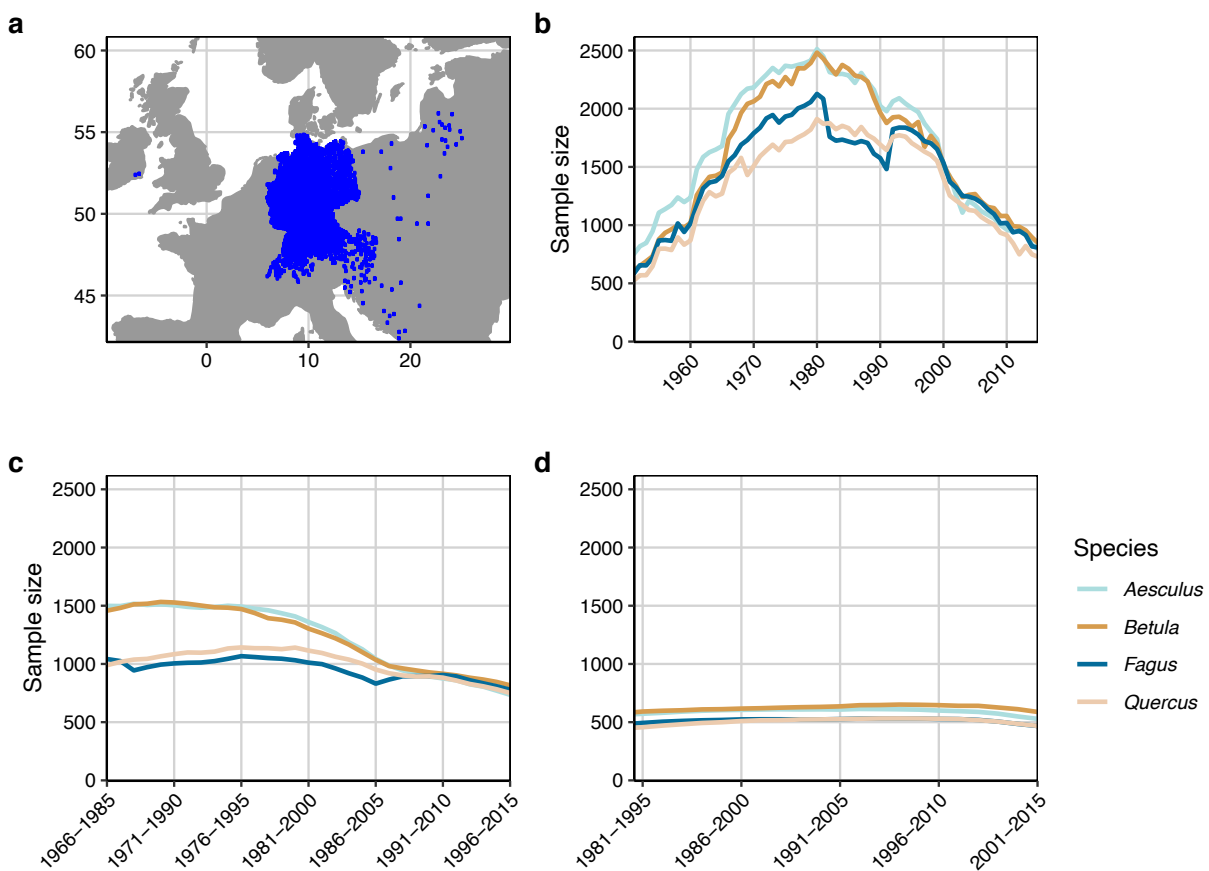
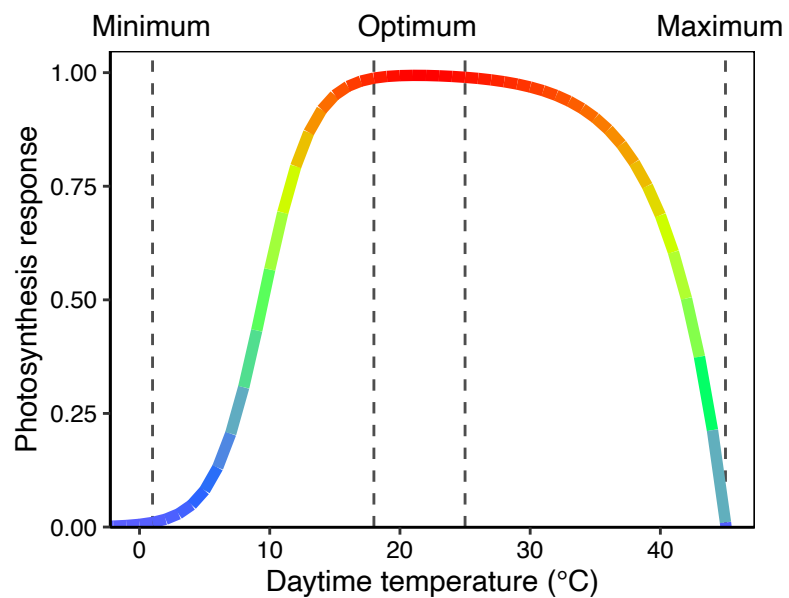


**Fig. S16. Total number of observations in the local PEP725 dataset. a,** Map of the PEP725 data sites. **b,** Total number of observations per year and species. **c,** Sample sizes of the long moving-window analysis (1966 to 2015), showing the yearly number of observations for each 20-year moving window period. **d,** Sample sizes of the short moving-window analysis (1980 to 2015), showing the yearly number of observations for each 15-year moving window.

261  
262  
263  
264  
265  
266  
267



268  
269  
270  
271  
272  
273  
274

**Fig. S17. Photosynthesis response to temperature as implemented in the LPJ photosynthesis model.** The minimum and maximum temperature threshold is 1°C and 45°C, respectively. The temperature optimum ranges from 18° to 25°C. Following ref<sup>48</sup>, this response curve reflects the photosynthesis optimum at latitudes between ~35–60°N.

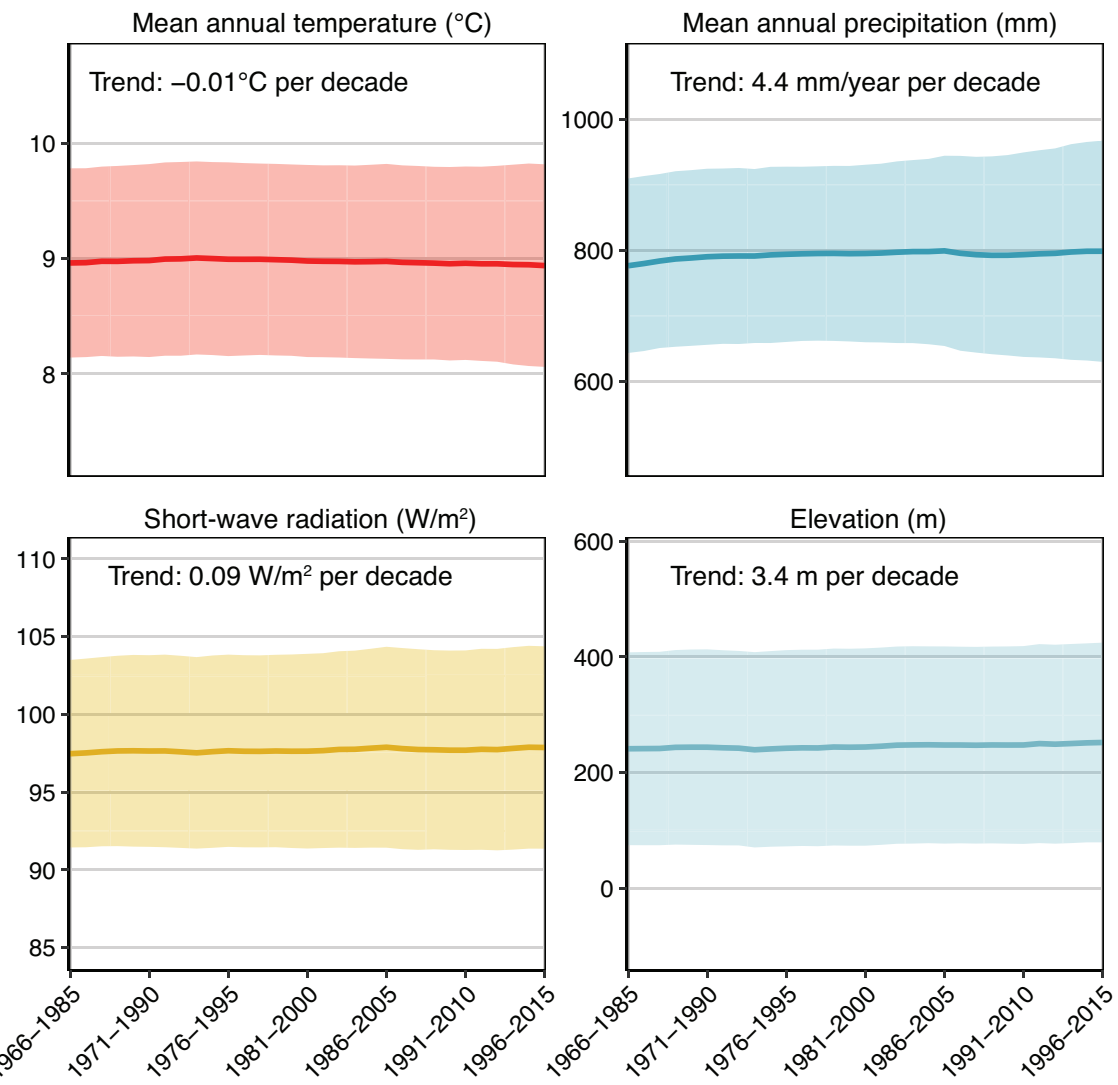


**Fig. S18. Average climate and elevation of the European PEP725 sites included in each 20-year moving window.** Climate refers to the 1948–2015 means of mean annual temperature, mean annual precipitation, and short-wave radiation. To test for possible differences in the average climate conditions between moving windows as a result of variations in the sites included in each window, we first obtained the mean of the 1948 to 2015 climate for each site, and then calculated the average  $\pm$  standard deviation for all sites included in each moving-window interval. On average, the 1948 to 2015 mean of the mean annual temperature of the sites included in each window decreased by only  $0.01^{\circ}\text{C}$  per decade, mean annual precipitation increased by  $4.4 \text{ mm/year}$  per decade, short-wave radiation increased by  $0.09 \text{ W/m}^2$  per decade, and elevation increased by  $3.4 \text{ m}$  per decade. These results show that there is no systematic bias in the average site-level climate conditions among moving windows.

275  
276  
277  
278  
279  
280  
281  
282  
283  
284  
285  
286